ON THE CONNECTION BETWEEN METAL ABSORBERS AND QUASAR NEBULAE

Doron Chelouche[1,2], Brice Ménard[3,1], David V. Bowen[4], and Orly Gnat[5]

Draft version August 3, 2021

ABSTRACT

We establish a simple model for the distribution of cold gas around $L^\star$ galaxies using a large set of observational constraints on the properties of strong Mg II absorber systems. Our analysis suggests that the halos of $L^\star$ galaxies are filled with cool gaseous clouds having sizes of order 1 kpc and densities of $\sim 10^{-2}$ cm^{-3}. We then investigate the physical effects of cloud irradiation by a quasar and study the resulting spectral signatures. We show that quasar activity gives rise to (i) extended narrow-line emission on ~ 100 kpc scales and (ii) an anisotropy in the properties of the absorbing gas arising from the geometry of the quasar radiation field. Provided that quasars reside in halos several times more massive than those of $L^\star$ galaxies, our model predictions appear to be in agreement with observations of narrow emission-line nebulae around quasars and the recent detections of ~ 100 kpc cold gaseous envelopes around those objects, suggesting a common origin for these phenomena. We discuss the implications of our results for understanding absorption systems, probing quasar environments at high redshifts, and testing the quasar unification scheme.

Subject headings: atomic processes — galaxies: halos — quasars: absorption lines — quasars: emission lines

1. INTRODUCTION

Observational data on quasar absorption lines indicates that $L^\star$ galaxies are surrounded by cool ($\sim 10^4$ K) gas condensations ranging up to radii of $\sim 100 h_{70}^{-1}$ kpc[6] (Bergeron et al. 1987, Steidel et al. 1995, Churchill et al. 2005, Zibetti et al. 2006). Similar distributions have recently been found around quasars (Bowen et al. 2006, 2007). In addition, several teams have discovered that bright quasars are surrounded by giant line-emitting nebulae observed at transitions such as Lyα (e.g., Wampler et al. 1975, Heckman et al. 1991a,b, Christensen et al. 2006). In this paper we investigate whether the two phenomena could originate from the same type of gas clouds around galaxies thereby connecting gas absorption and line emission in galaxy and quasar halos.

Quasar spectra have historically been a main source of information about large scale matter distribution in the universe. Such information has been obtained by studying absorption lines induced by intervening material between us and the quasar. In the optical wavelength range, absorption lines by metal-enriched gas at $z \lesssim 2$ originate from low to moderate-ionization species and the easiest feature to detect is usually the Mg II doublet ($\lambda\lambda 2796.35, 2803.53$). It is the first resonance transition of an abundant element with a large oscillator strength to enter the optical range and has therefore been the most commonly used tracer of cool gas. Several studies have shown that Mg II arises in gas spanning more than five orders of magnitude in neutral hydrogen column density, from $N_{\rm HI} \simeq 10^{17} - 10^{22}$ cm^{-2} (Bergeron & Stasinska 1986; Steidel & Sargent 1992; Churchill et al. 2000). Following the

suggestion by Bahcall & Spitzer (1969) that quasar absorption lines might arise in halos around galaxies, an association between absorbers and galaxies has been reported, starting from small samples of a few to ~ 50 galaxies (Bergeron 1986; Cristiani 1987; Bergeron & Boisse 1991; Steidel et al. 1997; Churchill et al. 2005) to statistical measurements involving thousands of objects (Zibetti et al. 2005 & 2006, Ménard et al. 2007).

While a connection between galaxies and metal absorbers has been firmly established, the origin of the absorbing gas remains unclear. Whether these absorption line systems trace gas being accreted by a galaxy or outflowing from it is still a matter of debate. Among the possible origins for absorption line systems in galaxy halos are condensations of cool clouds from hot and dilute halo gas via thermal instability (e.g., Mo & Miralda-Escude 1996, Maller & Bullock 2004), cool gas that is bound to dark matter sub-halos embedded within the main halo (e.g., Sternberg, McKee, & Wolfire 2002 and references therein), and starburst driven winds from galaxies (e.g., Oppenheimer & Davé 2006, Prochter et al. 2006). Additional explanations include (warped) galaxy disks (Bowen et al. 1995, Prochaska & Wolfe 1998) as well as low surface brightness companion objects (York et al. 1986, Petitjean & Bergeron 1994).

Some galaxies contain active nuclei and it is thought that all quasars are harbored in galaxies. The properties of quasar hosts are not well characterized but it is believed that bright quasars are usually harbored in rather massive, star-forming galaxies ranging from ~ 1 to $\sim 30 L^\star$ (Jahnke & Wisotzki 2003). Little is known about the environments of quasars, with recent studies suggesting that brightest objects live in somewhat over-dense environments (Serber et al. 2006). Like galaxies, the immediate environment of quasars can also be probed in absorption: using a survey of projected quasar pairs from the *Sloan Digital Sky Survey* (SDSS) our team has recently showed that quasars, like galaxies, are surrounded by Mg II gas on scales ranging up to $100 h_{70}^{-1}$ kpc (Bowen et al. 2006). Using a larger sample of quasar pairs, we have now found that the transverse gas distribution around quasars, as traced by Mg II, suggests a covering factor of order unity up

[1] School of Natural Sciences, Institute for Advanced Study, Einstein Drive, Princeton 08540, USA; doron@ias.edu

[2] Chandra Fellow

[3] Canadian Institute for Theoretical Astrophysics, University of Toronto, 60 Saint George Street, Toronto, ON M5S 3H8, Canada

[4] Department of Astrophysical Sciences, Princeton University, Princeton, NJ 08544

[5] School of Physics and Astronomy and the Wise Observatory; Tel-Aviv University, Tel-Aviv, Israel

[6] Throughout the paper we use $H_0 = 70 h_{70}$ km s^{-1}Mpc^{-1}, $\Omega_M = 0.7$, and $\Omega_\Lambda = 0.3$.

to $\sim 100\,h_{70}^{-1}$ kpc (Bowen et al. 2007).

Gas which is associated with the quasar environment is also commonly observed (via resonance line absorption such as C IV $\lambda 1548$) in our line-of-sight toward quasars and is identified by its proximity (within $\sim 10^3$ km s^{-1}) to the quasar redshift. Nevertheless, it is generally hard to establish whether such gas lies in the vicinity of the black hole (on sub-pc scales) or whether it originates in its host galaxy or its surrounding halo (see Crenshaw et al. 2003 for a review).

Deep imaging and spectroscopic observations of quasars reveal that a significant fraction of them have surrounding emission-line nebulosities extending out to $\sim 100\,h_{70}^{-1}$ kpc. Such nebulosities are often detected in Lyα emission (e.g., Heckman et al. 1991, Christensen et al. 2006) or the [O III] $\lambda 5007$ line (Stockton & MacKenty 1987, Fu & Stockton 2006) with recent surveys suggesting that radio-loud quasars (RLQ) may have brighter Lyα nebulosities (Christensen et al. 2006). Little is known about the physical nature of these nebulae and various scenarios pertaining to both gas accretion onto the quasar as well as gas ejection from it have been put forward as possible explanations (e.g., Heckman et al. 1991, Haiman & Rees 2001).

Motivated by these recent findings, we investigate in this work whether the emitting gas seen around quasars is consistent with being the same material as that observed around galaxies (and quasars) in absorption. The paper is organized as follows: In §2 we first summarize some observational constraints on the properties of cool gas around galaxies used to calibrate our model. A geometrical model is then constructed and its physics is discussed. We then (§3) use this model to study the effects on the absorption and emission properties of halo gas when exposed to a quasar radiation field. In addition, we show that such a model can naturally explain the distribution of cool gas around quasars and the existence of large-scale Lyα emitting nebulae. We discuss the implications of our results for galaxy formation, baryon fraction in the Universe, and quasar physics in §4. Summary follows in §5.

2. THE DISTRIBUTION OF COOL GAS AROUND $L^\star$ GALAXIES

2.1. *Observational constraints from Mg II absorbers*

Observational data on Mg II absorption lines have provided a number of constraints on the spatial distribution and characteristics of the cool gas around galaxies. Here we list the most relevant results that can be used to model the Mg II distribution in the halo of an $L^\star$ galaxy:

1.) Strong Mg II systems, defined with a rest equivalent width $W_0 > 0.3$Å, inhabit the halos of $\sim L^\star$ galaxies, as was found by Steidel et al. (1997). These authors found that Mg II selected galaxy luminosities lie in the range $0.3 - 5 L^\star$ with a mean $\langle L \rangle \simeq 0.8 L^\star$. Their results also suggested a unit covering factor up to $\sim 50\,h_{70}^{-1}$ kpc and the absence of strong Mg II absorption on larger scales. More recent studies (Zibetti et al. 2005 & 2006, Churchill et al. 2005) indicate that strong Mg II absorption can actually be detected on scales reaching more than $100\,h_{70}^{-1}$ kpc but that the covering factor falls off in this range. We note that the study done by Zibetti et al. (2006) implies little evolution in the properties of absorbing galaxies up to $z \sim 1$.

2.) Strong Mg II absorbers usually show saturated absorption lines (as implied by the doublet ratio). High-resolution spectroscopy reveals that strong systems usually break into several kinematically distinct components (e.g., Churchill & Vogt 2001). When resolved, the widths of these components are consistent with gas at a temperature of $\sim 10^4$ K (e.g., Lanzetta & Bowen 1990). It has been established that the rest equivalent width of strong systems is roughly proportional to the number of distinct kinematical components. Bergeron & Petitjean (1990) found the relation between total rest equivalent width and number of clouds to be $W_0(\mathrm{Mg\,II}) \simeq 0.3 \times N_c$ Å and Churchill (1997) reported $W_0(\mathrm{Mg\,II}) \simeq 0.07 \times N_c$ Å where N_c is the number of clouds along the line-of-sight. If the individual clouds observed in these systems are relatively similar, then these results suggest that, even if the rest equivalent width of Mg II systems is mostly driven by a velocity dispersion, it can be used as a proxy for the number of clouds along the line of sight.

3.) Constraints on the sizes of Mg II systems have been obtained by studying the spectra of strongly lensed quasars. Limits on the size of individual absorption components are obtained by comparing absorption features across different lines of sight. Typical values span the range $0.1 - 10$ kpc for Mg II clouds (e.g., Rauch et al. 2002, Ellison et al. 2004) and perhaps somewhat larger sizes for systems detected by high ionization lines such as C IV $\lambda\lambda 1548, 1550$. At present this is the only direct means for estimating the size of cool gaseous clouds in galaxy halos (for an indirect method relying on photoionization modeling see e.g., Ding et al. 2003).

4.) Finally, HI measurements show that strong Mg II systems with $W_0 \sim 0.5$Å give rise to HI column densities in the range 10^{18-20} cm^{-2} while stronger systems with $W_0 \sim 2$Å have $N_{\mathrm{HI}} \sim 10^{19-21}$ cm^{-2} (Rao et al. 2006). Emission-based results from 21 cm surveys at $z = 0$ (Zwaan et al. 2005) indicate that the contribution of galaxy *disks* to the observed HI column density distribution can be substantial within ~ 20 kpc for certain orientations. (See also Bowen et al. 1995 and Prochaska & Wolfe 1997). However, on larger scales, the contribution of halo gas clouds is in general expected to dominate the HI column density distribution. The lack of correlation between Mg II absorption properties and galaxy size or inclination further supports this assertion (Steidel et al. 2002; see also Kacprzak et al. 2007).

2.2. *Modeling the spatial distribution*

We now introduce a simple phenomenological model aimed at reproducing the main aspects of the observational constraints presented above, namely the spatial extent of the gas, the cross-section for strong Mg II absorption and the distribution of hydrogen column densities observed around $\sim L^\star$ galaxies. We emphasize that, in this study, we do *not* attempt to investigate the physical origin of the gas, i.e. whether it is bound to satellite dark matter halos, infalling or being ejected out of the galaxy via winds. We consider a case in which the total mass density (baryonic and dark matter) for such a system is described by an isothermal profile:

$$\rho(r) = \frac{\sigma^2}{2\pi G r^2}, \quad r \le r_v = \frac{\sigma}{\sqrt{50}\,H_0} \tag{1}$$

where σ is the velocity dispersion, r_v the virial radius, and ρ is the density. The mass within a given radius r is then given by

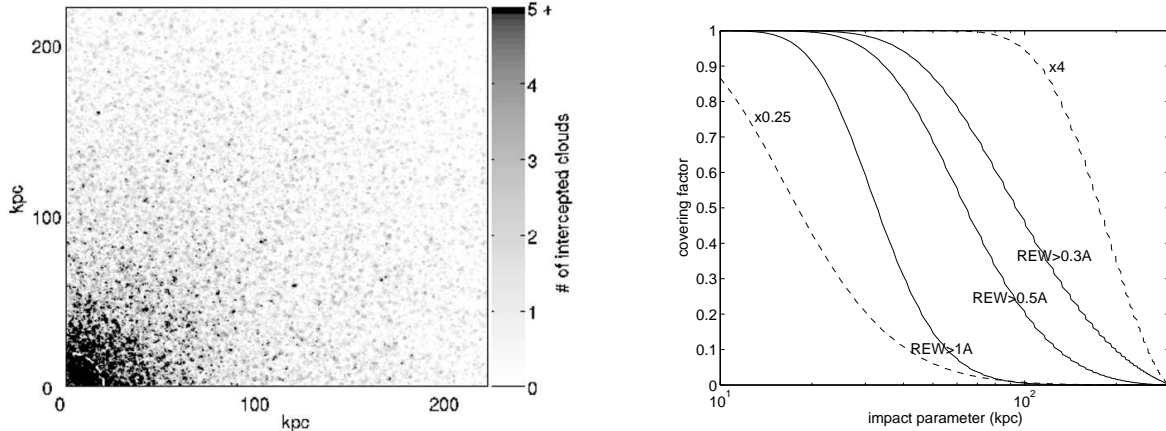$$M(<r) = \frac{2\sigma^2 r}{G} \tag{2}$$

FIG. 1.— The number-count distribution of Mg II clouds along different lines-of-sight through a halo of an $L^\star$ galaxy (see text). Note the increase in the number of intercepted cloud with decreasing impact parameter. Note also that clouds are distributed up to the virial radius though the probability for intercepting them on large scales is small. *Right:* The covering factor for strong Mg II absorption around galaxies. The different solid lines correspond to model predictions of the covering factor for different W_0 limits (denoted to the right of each curve) around an $L^\star$ galaxy. As shown, the covering factor for strong, $W_0 > 0.5$Å absorption is below 50% for impact parameters greater than 50 kpc. Conversely, weak absorption with $W_0 < 0.3$Å is common for impact parameters greater than 70 kpc. The dashed lines are model predictions for galaxy halo models with cool gas mass 0.25 and 4 times that of an $L^\star$ galaxy and for $W_0 > 0.5$.

and by definition, the density enclosed within the virial radius is 200 times the critical density. According to Fukugita & Peebles (2006), the one-dimensional mass-weighted velocity dispersion for late type galaxies is $\sigma_{\text{late}} = 140\,\text{km}\,\text{s}^{-1}$ which corresponds to a virial mass $M_\star \simeq 2.5 \times 10^{12} M_\odot$ within $r_v = 282\,\text{kpc}$.

For simplicity we assume that the cool gas around $L^\star$ galaxies is of the form

$$\rho_{\text{cool}}(r) \propto r^{-2}. \tag{3}$$

Such a density profile arises naturally in a wide range of models for the origin of the absorbing gas. In particular, it characterizes gas which follows the dark matter distribution in isothermal halos. It also a property of mass conserving outflowing winds or infalling gas (in spherical geometry) that holds over a range of radii where the velocity is roughly constant. As we shall later see, deviations from this power-law do not significantly affect our conclusions.

The multiple components observed in high-resolution spectra indicate that the gas does not follow an overall smooth distribution but is distributed in discrete systems. To reproduce this property, we consider the cool gas to be in the form of clouds that are distributed within the halo following a Poisson distribution with a mean number density, n_{cloud} following $\rho_{\text{cool}}(r)$. Considering a line-of-sight through the gaseous halo of a galaxy, the number of clouds intercepted along a physical path l is

$$dN_{\text{cloud}} = n_{\text{cloud}}(\mathbf{r})\,\pi R_{\text{cloud}}^2\,d\mathbf{l}, \tag{4}$$

where πR^2 is the cloud cross-section for inducing Mg II absorption, $\mathbf{r}$ is a vector from the halo center, and $d\mathbf{l}$ is measured along the line-of-sight. By integrating over the density profile of the gas we find the number of clouds along a given line-of-sight at some impact parameter, b, to be

$$N_{\text{cloud}}(b) = \frac{\pi}{2}\Psi(r_v/b) \times n_{\text{cloud}}(b)\,\pi R^2\,b \tag{5}$$

where $\Psi(r_v/b) = (2/\pi)\int_1^{r_v/b} d\xi\,\xi^{-1}/\sqrt{\xi^2 - 1}$.

As mentioned above, the overall rest equivalent width of strong Mg II systems is roughly proportional to the number of

subcomponents. We can therefore use this empirical relation and approximate the rest equivalent width of a Mg II absorber by

$$W_0 \simeq N_{\text{cloud}}W_c \tag{6}$$

with $W_c = 0.2$Å. Here we have used the mean of the proportionality factors reported by Bergeron & Petitjean (1990) and Churchill et al (2003)

The final constraint needed for our model is the normalization of the overall amplitude. Steidel (1993) has shown that Mg II absorption with $W_0 \gtrsim 0.5$Å is found within ~ 50 kpc of $L^\star$ galaxies with a unit covering factor. This imposes a constraint on our model: $\langle W_0(r = 50\text{kpc})\rangle \simeq 0.5$Å. Given the previous relation, it implies that, on average, about two Mg II clouds are intercepted by a line-of-sight with an impact parameter of 50 kpc. More recent results by Zibetti et al. (2005) & Churchill et al. (2005) have shown that there in fact exists a continuous distribution of impact parameters up to more than 100 kpc and the data suggest that the covering factor is less than unity on those scales. We note that once the function $W_0(r)$ has been normalized at 50 kpc, the cloud-distribution of Mg II systems introduced above automatically reproduces the drop of the covering factor for absorption and allows absorbing clouds to be found on scales >100 kpc, as indicated by recent studies. We note that the scatter in $W_0(b) \propto N_{\text{cloud}}(b)$ is largely due to the relatively small number of clouds. Specifically, the standard deviation is given by $[1 + \sqrt{N_{\text{cloud}}(b) + 0.75}]W_c$ (Gehrels 1986) and is therefore considerable ($\Delta W_0/W_0 \lesssim 1$). Interestingly, a large scatter is also seen in the data yet its magnitude is poorly constrained due to small number statistics per galaxy luminosity bin (Steidel et al. 1993).

We now combine all the above properties and display the resulting cloud distribution in Fig. 1. The left panel shows the distribution of intercepted clouds of cool gas as a function of impact parameter as well as the expected scatter. The right panel presents, for different absorption line sensitivities, the covering factor for absorption around $L^\star$ galaxies. We note that the observational constraints we are using are valid on scales greater than ~ 20 kpc. This is denoted in Fig. 1 by the
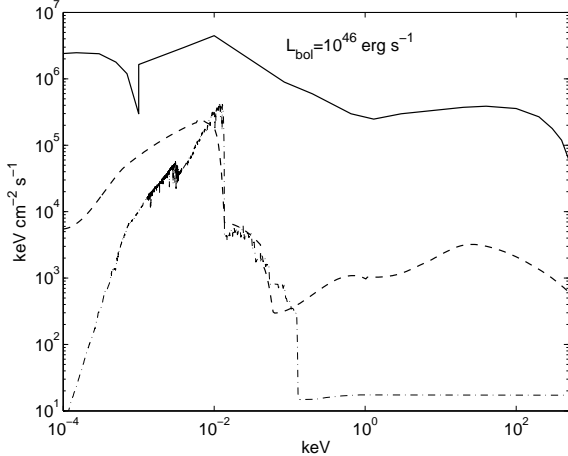
FIG. 2.— The various components of the ionizing radiation field considered in this work. The quasar spectral energy distribution (solid line), the galaxy ionizing radiation field (dash-dotted line), and the UV/X-ray background radiation field (dash line). The relative normalizations of the different components were scaled to the values that would be measured at a distance of 50kpc from the center of the galaxy (see text).

FIG. 3.— A contour plot of the Mg II $\lambda 2796$ optical depth (blue contours) and the H I column density (red contours), both in logarithmic units, as a function of the cloud particle number density and total hydrogen column density. Only the UV/X-ray ionizing background radiation is assumed. Lines corresponding to several cloud sizes are also drawn (see text).

white dashed circle. On scales smaller than 20 kpc, the contribution from the disk of late-type galaxies becomes important. In this paper we are only interested in gas distribution in the halo and we will focus only on these larger scales.

2.3. *Properties of Mg II clouds*

We now investigate the possible range of physical conditions which allow the existence of Mg II clouds around a galaxy. Given the low gas temperatures associated with individual Mg II absorption components, we neglect the effect of collisional heating by shocks, conduction, and cosmic ray heating (e.g., Bergeron & Stasinka 1986, Charlton et al. 2000) and only consider the effects of photoionization. For clouds in a galactic halo, most of the ionizing flux originates from the meta-galactic field (Haardt & Madau 1996) and the central galaxy. Contributions to the mean ionizing photon flux from satellite galaxies and other diffuse sources can be neglected. The background UV/X-ray ionizing radiation is due to quasars and stars. Characterizing this spectrum requires knowledge of the star formation rate and quasar activation history as well as the opacity of intervening material. In this work we use the Haardt & Madau (1996) calculations and consider the background radiation at $z \sim 1$. The spectrum, integrated over 4π steradians, is shown in Fig. 2 with a dashed line.

In addition to diffuse background radiation there is also the ionizing radiation from the central galaxy. We model the galaxy spectrum using the Bruzual & Charlot (1996) models and the Chabrier (2003) initial mass function. We assume grey opacity beyond the Lyman edge so that 5% of the ionizing continuum escapes to the halo (e.g., Bland-Hawthorn & Maloney 2001). A population of X-ray binaries is also included (Norman et al. 2004) using the infra-red to X-ray scaling of Ranalli et al. (2003). The galaxy ionizing radiation is shown in Fig. 2.

To model the photoionization and thermal equilibrium of the cool gas clouds in the halo, we use the CLOUDY c06.02a photoionization code (Ferland et al. 1998) with the Badnell di-electronic recombination coefficients (Badnell 2006). We
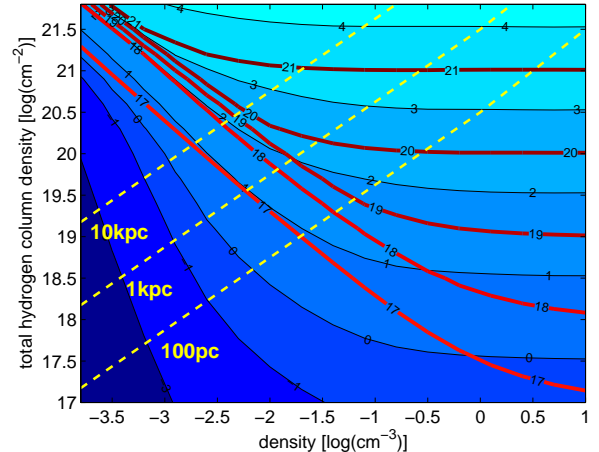
simplify the calculations by assuming a slab geometry with one surface of the cloud exposed to half of the total ionizing flux. Photoionization calculations are carried out to the center of the cloud and symmetry is assumed when calculating the total column density of ions (see Gnat & Sternberg 2004 for a more realistic treatment of the problem). We assume the gas composition to be $0.1\times$solar (Turnshek et al. 2005, York et al. 2006).

We investigated several possible scenarios for the structure of the clouds: (a) constant density; this is perhaps the simplest model yet has been the main route by which a wide range of astrophysical phenomena are modeled, (b) constant radiation and gas pressure; this may be relevant to clouds in pressure equilibrium with their surroundings (e.g., with the inter-cloud medium), (c) constant temperature; this could be envisioned as gas which is collisionally heated to the virial temperature of dark matter minihaloes. Given the parameter space of interest, it appears that the different models do not give appreciably different results. For clarity we will show only the results obtained for a constant density medium.

We have calculated the column density of Mg II and H I as a function of cloud hydrogen (ionized and neutral) column density and the number density of particles. The results are shown in Fig. 3.

We have repeated the calculations including the effect of the ionizing radiation field of the galaxy and found it to be dominant within the central $\sim 40\,\mathrm{kpc}$ (see §2.4 for the effect of cloud shielding). The gas considered here, having a low ionization level, is sensitive to the ionizing flux just above the Lyman edge. To first order, gas which is exposed to the galaxy ionizing flux (in addition to the UV ionizing radiation flux, f_{UV}), f_g would attain a similar ionization structure to that shown in Fig. 3 provided its density is greater by a factor $1 + f_g/f_{UV}$. Similarly, at higher redshifts, where the UV background radiation is stronger the density of a cloud with a similar ionization level to that shown in Fig. 3 would be higher by the UV flux ratio of the epochs.

Constraining the parameter range relevant to strong Mg II absorbers is not straightforward since strong Mg II lines are usually saturated and additional observational constraints are needed to estimate their typical density and column density. A
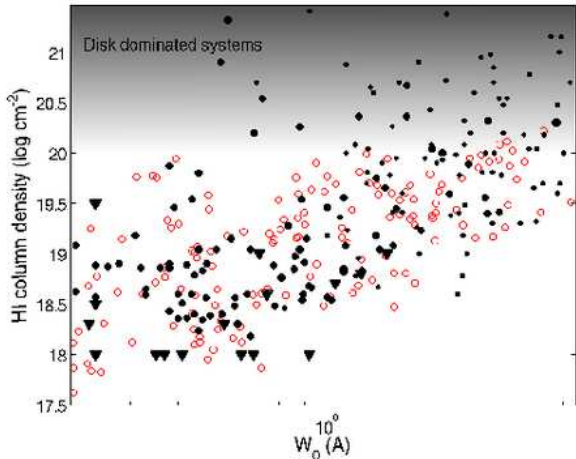
FIG. 4.— HI column density vs. the rest equivalent width of Mg II for Mg II selected systems (see Rao et al. 2006). Data appear as black points with upper limits marked by triangles. Different point size indicates different selection criteria employed by Rao et al. (large points are systems selected by criteria 1-2 while smaller points by 3-4; see Rao et al. 2006); both sets of points have similar properties for the low column density range considered here. The contribution of galaxy disks to the measured H I column density may become important in the shaded region of the diagram (Zwaan et al. 2005) and our model does not attempt to account for it. The simulated data are drawn in red points and reproduce the lower column density envelope (see text).

useful constraint is the size of the clouds derived from strong lensing studies. As noted above, such studies indicate that the size of Mg II absorbers is ~ 1 kpc. This constraint substantially reduces the relevant parameter space in Fig. 3. A second constraint comes from the H I column density measurements for strong absorbers (Rao et al. 2006). Using the rest equivalent width as a proxy for the column density along the line-of-sight (see eq. 6) we see from Fig. 4 that a typical cloud has an H I column density of $\sim 10^{18}$ cm^{-2}, implying a density of about 2×10^{-2} cm^{-3}. Such values are consistent with previous estimates in the literature for the density of cool gas in galaxy halos (e.g., Sternberg, McKee, & Wolfire 2002 for the case of high velocity clouds in the Galaxy).

The scatter in the N_{HI} vs. W_0 relation presented in Fig. 4 is significantly larger than that of the simplified model presented in the previous section. Several effects not included in our model could also contribute to this scatter: a distribution of galaxy masses, types, star formation histories, etc. – all of which are beyond the scope of this paper and are not observationally motivated at this stage. In the absence of a clear physical motivation, we attempt to take this effect into account by introducing a distribution of cloud sizes (as implied by the observations; §2.1). Here, clouds have similar densities which allow them to be in pressure equilibrium with their environment. (We find the alternative scenario in which all clouds have the same size but different densities less plausible since the implied evaporation times would be embarrassingly short compared to the Hubble time; see appendix.) To this end we assume that the size of individual Mg II clouds is drawn from an intrinsic distribution $\phi(R_{cloud})$ so that observed one (taking into account cloud cross-section effects on the detectability rates) $\phi_{obs}(R_{cloud}) \propto \phi(R_{cloud}) \times R_{cloud}^2$. A simple power-law distribution gives a reasonably good description of the data:

$$\phi(R_{cloud}) \propto R_{cloud}^\beta, \quad \text{with} \ R_{cloud}^{min} < R_{cloud} < R_{cloud}^{max}, \quad (7)$$

which implies a mass distribution:

$$\phi(M_{cloud}) \propto M_{cloud}^{(\beta-2)/3}, \ \text{with} \ M_{cloud}^{min} < M_{cloud} < M_{cloud}^{max} \ (8)$$

where M_{cloud} is the mass of a single cloud. This distribution is defined between some minimum and maximum sizes. We generate a population of clouds as follows: in each rest-equivalent width bin we randomly picked the sizes of N_{cloud} clouds drawn from ϕ and calculated their ionization structure and their H I column densities. The total H I column of all clouds was then summed taking into account the scatter caused by intercepting a spherical cloud at various positions. This procedure resulted in one simulated point in Fig. 3 which was then repeated covering the entire rest-equivalent width range spanned by the data. As we are only interested in modeling the gas contribution originating from the halo of a galaxy, we do not model the high HI column density values with $N_{HI} > 10^{20}$ cm^{-2} and for which a disk is a likely contributor (Zwaan et al. 2005). We note that our estimates for the total mass of cool gas in the halos of galaxies will change by a factor of order unity by including the upper end of the column density distribution in our model. Given our density estimates from photoionization calculations and the constraints on the mean size of clouds then a good fit for the Rao et al. dataset is obtained for $R_{cloud}^{min} = 0.3$ kpc, $R_{cloud}^{max} = 1.5$ kpc and $\beta = -2.5$ (corresponding to $\beta = -0.5$ for the observed distribution). Our approach allows us to reproduce the main observational trends summarized in Fig. 4.

The gas temperature in our model is $\sim 10^4$ K and so the gas pressure $P/k_B \sim 200$ cm^{-3} K (i.e., similar to the value used by e.g., Mo & Miralda-Escude 1996 and Gnat & Sternberg 2004 but somewhat lower than that implied by Fukugita & Peebles 2006). The implied cloud mass distribution, $\phi(M_{cloud}) \propto M_{cloud}^{-1.5}$, with $M_{cloud}^{min} = 6 \times 10^4$ M$_\odot$ and $M_{cloud}^{max} = 7 \times 10^6$ M$_\odot$. Clouds are Jeans stable provided that the total mass (dark and baryonic matter) is $M_{cloud} < 10^8$ M$_\odot$. The clouds are also relatively stable with respect to hydrodynamic instabilities (such as Klevin-Helmholtz) and evaporation (Maller & Bullock 2004).

It is interesting to note that our typical Mg II absorbing cloud hydrogen is mostly ionized. Most of the metals are in singly or doubly ionized configuration. Nevertheless, the large total gas columns result in higher ionization levels having a non-negligible column density. Specifically, the column density of C IV in our model can exceed 10^{13} cm^{-2} which translates to an optical depth of order unity and is therefore consistent with a picture in which C IV and Mg II absorption have a common origin. The uniform density, cool clouds considered here cannot account for the strong intervening O VI $\lambda 1035$ systems (see Danforth & Shull 2005, Bergeron & Herbert-Fort 2005) and an additional component/physics is required to explain them (e.g., Mo & Miralda-Escude 1996, McKee & Begelman 1990 and references therein).

In our analysis we have assumed that all clouds are exposed to a similar flux level regardless of their location in the halo. Nevertheless, the effect of shielding of the ionizing flux by other clouds could be, in principal, important. To estimate the magnitude of this effect let us consider a cloud located 50 kpc from the galaxy. Such a cloud would see an effective column density of a few $\times 10^{18}$ cm^{-2} (corresponding to a few clouds). When shielding is included as well as the contribution from the central galaxy, we find an overall decrease in the photoionization rate by a factor ~ 2 compared to the non-
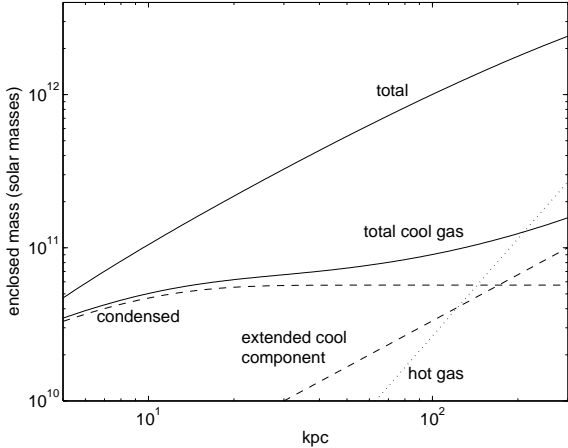
FIG. 5.— The extended cool gas component considered in this work within the framework of the massive corona model by Fukugita & Peebles (2006; see their paper for the assumptions and physical motivation behind each component). The total mass in cool gas is comparable to that of the hot component within the virial radius. Given the condensed form of the extended cool component it occupies only a small fraction ($\sim 1\%$) of the entire volume.

TABLE 1
MODEL SUMMARY

Cloud parameters	
Gas mass	$6 \times 10^4 < M_{cloud} < 7 \times 10^6 M_{\odot}$
Radius	$0.3 < R_{cloud} < 1.5$ kpc
Density	$\rho_{cloud} = 0.02$ atom cm^{-3}
Metallicity	$0.1 Z_{\odot}$
Halo parameters (20 kpc $< r < r_v$)	
Cool gas density profile	$\rho \propto r^{-2}$
Dark matter velocity dispersion	$\sigma = 140$ km/s
Virial radius	$r_v = 282$ kpc
Virial mass	$M \simeq 10^{12} M_{\odot}$
Cool gas Mass[a]	$M_{cool} \sim 10^{11} M_{\odot}$
Number of clouds[a]	$\sim 7 \times 10^4$

[a] for a covering factor of unity and within r_v (see section 2.4)

shielded case.

2.4. *Summary & limitations of the model*

As stated above, our model is aimed at providing a framework for studying the effects of a quasar radiation field on the absorption and emission properties of the corresponding system. We have calibrated it using observational constraints on the spatial distribution of Mg II clouds within the halo of $\sim L^{\star}$ galaxies and the corresponding HI column densities, and using photoionization calculations we have shown that the implied cloud parameters are consistent with the existence of Mg II gas. We summarize the main model parameters in Table 1.

This model leads to a picture in which $L^{\star}$ halos are filled with gaseous clouds which are partially ionized and sufficiently optically thick to be detected in both low- and high-ionization (e.g., C IV) absorption lines. These clouds have sizes of order 1 kpc, masses of $\sim 10^6 M_{\odot}$ and particle densities $\sim 10^{-2}$ cm^{-3}, amounting to a cool gas mass of $\sim 10^{11} M_{\odot}$ *within the virial radius*, i.e. ~ 280 kpc.

The results presented above assume that cool gas clouds are

distributed throughout the entire volume of the halo up to the virial radius. Nevertheless, the virial radius has no clear physical connection to the scale, r_{cool}, up to which cool clouds exist. In particular, the value of r_{cool} is expected to depend on the (unknown) origin of the cool gas. For example, if the gas is ejected from the galaxy r_{cool} is likely to be smaller than the case in which cool gas is accreted from the inter-galactic medium. Moreoever, different values may be obtained if the cool gas condenses out of the virialized halo gas (e.g., Mo & Miralda-Escude 1996). At present, little is known with confidence about the origin of such cool gas and observations provide only very loose constraints, hence r_{cool} is ill-determined. That being said, we find that the mass of cool gas in galaxy halos depend relatively little on r_{cool} for the relevant scale range. Specifically, to reproduce the covering factor statistics on large scales, we obtain $M_{cool} \sim 3\,(4) \times 10^{10} M_{\odot}$ for $r_{cool} = 50\,(100)$ kpc. Clearly, the mass of cool gas in galaxy halos is considerable for all plausible values of r_{cool} and a covering factor of order unity. In what follows we therefore assume the gas occupies the entire virial volume (i.e., $r_{cool} = r_v$).

We note that, given our model assumptions and calibration constraints, the overall mass of cool gas, M, scales with the mean cloud size, $\langle R_{cloud} \rangle$ and is inversely proportional to the assumed gas density. It must be emphasized that the total mass of cool gas depends on the assumed covering for absorption, i.e. a quantity still debated in the literature. In the present study we have used a covering factor of unity for strong MgII absorption within ~ 50 kpc, as suggested by Steidel et al. (1997). However, other studies claim lower values (~ 0.2 from Bechtold & Ellingson (1992) and ~ 0.5 from Tripp & Bowen 2005). As the total mass of cool gas scales linearly with this quantity, we might be overestimating the mass if the actual covering factor is not unity.

According to our model, the mass of cool gas in galaxy halos scales linearly with halo size. Specifically, the mass within 30 kpc is $M_{cool} < 10^{10} M_{\odot}$ and, by extrapolation to smaller scales, is comparable to that estimated by Martin (2006) for ultra-luminous infrared galaxy outflows. In Fig. 2.4 we show the different components of the average mass profile of late-type galaxies proposed by Fukugita & Peebles (2006), and show that including the distribution of cool gas proposed in the present paper is only a modest departure from it.

So far we have concentrated on modeling the gas within the halo of an $L^{\star}$ galaxy with $M_{vir} = 2.5 \times 10^{12} M_{\odot}$. It is interesting to note that our model *may* be scaled to different galaxy luminosities and masses. Indeed, analyses by Steidel et al. (1997) and Guillemin & Bergeron (1997) have indicated that the normalization of the Mg II rest equivalent width follows a relation

$$W_0(r,L) = W_0(r) \times \left(\frac{L}{L^{\star}}\right)^{\gamma} \qquad (9)$$

with $\gamma \simeq 0.1 - 0.4$. Such a scaling has been reported in the luminosity range $0.3 - 5L^{\star}$ and at redshifts $0.5 < z < 1$. Extrapolating it further is therefore uncertain. The above relation may be understood within the framework of our model as a dependence of the number of clouds, hence mass of cool gas, on luminosity. Denoting the mass of cool gas in $L^{\star}$ galaxies by $M^{\star}$ then the mass of cool gas in halos of galaxies with luminosity L may be written as $M(L) = f_M(L)M^{\star}$ where f_M is a dimensionless scaling factor.
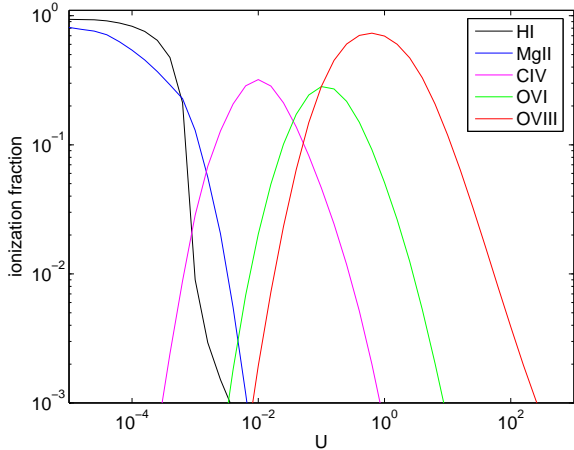
3. QUASAR HALOES

FIG. 6.— The ionization fraction of the abundant elements as a function of the ionization parameter, U. In this case the radiation field of the quasar overwhelms all other sources within $\sim 10 Mpc$ of the quasar. Gas with the same density and distance as a typical Mg II absorbing cloud would be highly ionized.

We now investigate the effects of a quasar on the gas distribution within a halo and discuss the observational signature in absorption and emission. Our main assumption is that quasar halos are analogous to those of non-active galaxies. As indicated by recent studies (e.g., Jahnke et al. 2004), the hosts of bright quasars seem to correspond to a few $\times L^\star$ galaxies. Furthermore, a recent study by Serber et al. (2006) seems to indicate that bright quasars reside in over-dense regions implying that their dark matter halos are several times those typical of $L^\star$ galaxies. Motivated by these studies we shall allow f_M to deviate from unity. We show below that many observational constraints may be accommodated by using $f_M \sim 5 - 10$ for the mass of cool gas in quasar halos.

3.1. *Thermal and Ionization Structure*

In what follows we compute the time-*independent* ionization and thermal structure of a cloud exposed to a constant quasar ionizing flux. In the Appendix we present time-*dependent* calculations and show that the steady-state assumption suffices for the luminosity range and the relevant spectral features considered here.

In modeling the spectral energy distribution (SED) of the quasar we have used the continuum defined by Sazonov, Ostriker, & Sunyaev (2004) which is shown in Fig. 2. Ionizing sources other than the quasar can be safely neglected. We start by introducing the ionization parameter, U, which is the ratio of photon density to particle number density and is a measure of the ionization level for photoionized gas. For the chosen SED we obtain that

$$U \simeq 0.6 L_{46} \left(\frac{n}{10^{-2}\,\mathrm{cm}^{-3}} \right)^{-1} \left(\frac{r}{50\,\mathrm{kpc}} \right)^{-2}. \quad (10)$$

where the quasar luminosity is $L = 10^{46} L_{46}$ erg s^{-1}. The ionization structure of several commonly detected ions as a function of U is shown in Fig. 6. By combining these results with the density estimates from our model (§2), we can compute the ionization level and temperature as a function of the radius from the center of the galaxy. The results for the temperature profile are shown in Fig. 7. As expected, the quasar has a substantial effect on the thermal state of the

inner parts of the halo and can heat the (initially cool) gas to high temperatures by means of photo-absorption. The extent to which the Mg II halo is ionized depends mainly on the quasar luminosity. For example, a quasar with $L_{46} = 1$ heats gas within the inner 20 kpc to some 10^5 K with gas at 50 kpc being ionized to a few $\times 10^4$ K. Objects with Seyfert-like luminosities ($L_{46} \lesssim 0.1$) have a smaller effect on their immediate environments and heat the gas within their inner 20 kpc to a few $\times 10^4$ K with clouds at larger radii remaining relatively cool. In contrast, very luminous quasars can heat their 100 kpc environment to temperatures of order 10^5 K with gas within the inner 10 kpc being able to reach the Compton temperature. The effect of a luminous quasar is not necessarily limited to halo gas and low density gas may be affected on much larger (Mpc) scales. Our calculations indicate (Fig. 6) that for clouds to remain relatively cool within the central 30 kpc of a $L_{46} = 1$ source, their density should be $\gg 10^2$ cm^{-3}, i.e. considerably higher than the values considered here and those thought to be representative of Mg II clouds (c.f., Stockton et al. 2002).

The ionization structure closely follows the temperature profile. Fig. 7 shows the ionization fraction of several ions as a function of radius in the halo for the case of $L_{46} = 1$. Clearly, gas within the inner 100 kpc is devoid of Mg II, with C IV O VI, and O VIII being most abundant; the ionization fraction of the latter peaking on the smallest scales. For a $f_M = 5$ halo with a $L_{46} = 1$ quasar (e.g., Jahnke et al. 2004 and equation 9), the gas remains optically thin above the Lyman edge. For different source luminosities the abscissa should be rescaled by L_{46}^{-1}. For low quasar luminosities ($L_{46} < 0.1$) even the inner regions of the halo remain at low temperatures and the gas is less affected by the quasar on ~ 100 kpc scales (see Fig. 7).

The active galactic nuclei (AGN) unification scheme (Antonucci 1993) suggests that quasars emit light in a double cone geometry with an opening angle θ (see Fig. 8). Such an anisotropy in the radiation field will be imprinted in the properties of the gas distribution around the quasar. In the next sections we discuss the observational implications, both in absorption and emission.

3.2. *Quasar-halo absorption properties*

Clouds of gas that lie within the ionization cone of the quasar would be heated and ionized, and would follow the ionization structure presented in Fig. 7. Therefore, the line-of-sight to a quasar would be largely devoid of associated Mg II absorption due to the halo clouds modelled in this paper. Nevertheless, such highly ionized clouds are expected to give rise to associated absorption features from species like H I, C IV, and O VI – depending on their ionization structure which is determined by the quasar luminosity and their distance from the source. In contrast, lines-of-sight probing the quasar halo at finite impact parameters from the quasar would intercept cool gas which is not affected by the quasar radiation field and is therefore likely to show absorption features due to low ionization species as those seen around non-active galaxies. The number of Mg II clouds intercepted by a given sight-line depends not only on the total number of clouds within the halo (which, for non-active galaxies, depends on the galaxy luminosity; see equation 9) but also on the opening angle of the quasar.

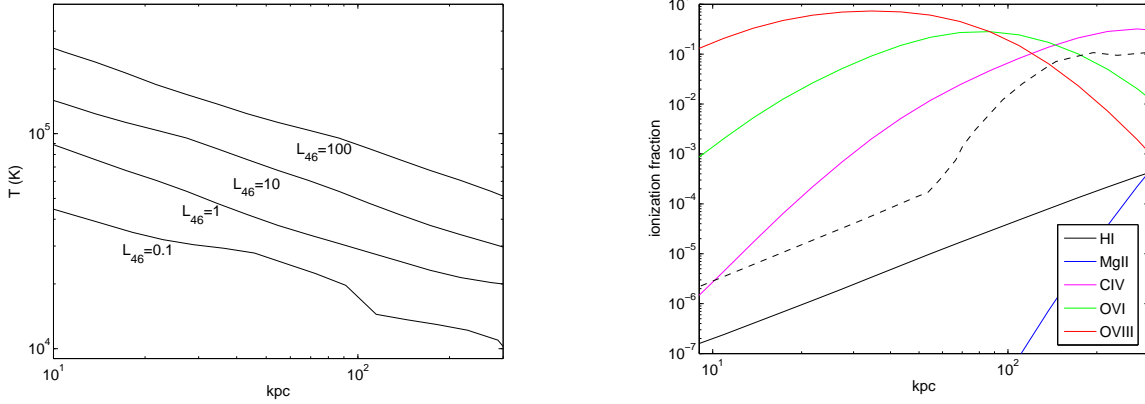Given the above model, we now discuss the observable

FIG. 7.— The thermal and ionization properties of halo gas ($f_M = 5$) illuminated by a quasar. *Left:* The temperature profile for a constant density, optically thin medium with density of $0.02\,\mathrm{cm}^{-3}$ (see text) for several values of quasar luminosity. Clearly, the temperature drops with distance as the ionization parameter decreases ($\propto r^{-2}$). The radiative effect of Seyfert galaxies on their environment is more localized than that of bright quasars. *Right:* The ionization structure as a function of distance from a $L_{46} = 1$ quasar. As expected, the ionization level decreases with distance due to the dilution of the radiation field. The fraction of Mg II recovers only on Mpc scales while closer to the quasar (on $\sim 100\,\mathrm{kpc}$ scales) C IV is expected to show absorption signatures while on smaller scales still ($\sim 20\,\mathrm{kpc}$) O VI would show up in the spectrum. The gas is very highly ionized within $\sim 30\,\mathrm{kpc}$ and could be detected in the X-rays. For quasars with different luminosities the abscissa should be rescaled by $L_{46}^{1/2}$. Thus, brighter quasars would ionize their environment to larger distances. The dashed line corresponds to the ionization fraction of H I for the case of $L_{46} = 0.1$. The hump beyond $\sim 50\,\mathrm{kpc}$ is the result of self-shielding (see text).
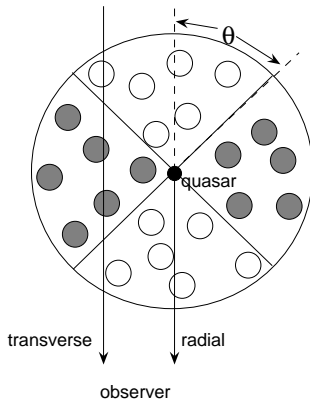

FIG. 8.— The geometry considered here whereby a quasar emits ioniz-ing radiation into a cone with opening angle θ. Cool gas clouds which are exposed to the ionizing radiation (circles) are heated while those that are shielded from the ionizing radiation remain cool (filled circles) and their properties resemble those of halos associated with non-active galaxies. Off-center lines of sight will intercept cool gas in the transverse direction, while those that point radially toward the quasar will mostly see ionized gas (see text).
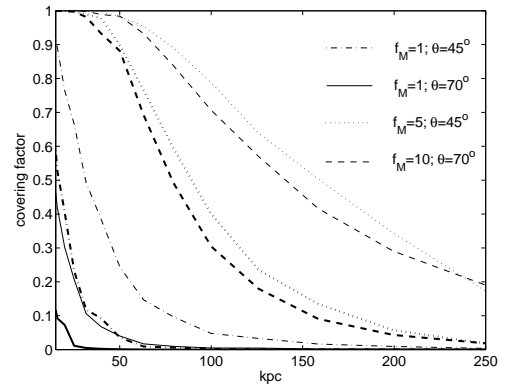

FIG. 9.— The covering factor for strong Mg II absorption as a function of the impact parameter for lines-of-sight passing through the halo of a quasar (see figure 8). Thick (thin) lines correspond to the covering factor for systems with $W_0 > 1$Å ($W_0 > 0.6$Å). Four halo models are considered that differ by the mass of cool gas within the virial radius (denoted by f_M; see text) and the opening angle, θ, of the quasar radiation field. As expected, the covering factor declines with increasing impact parameter due to the decreasing cloud density with distance. The covering factor for strong absorption is sensitive to both θ and f_M. As θ increases, more gas is ionized and the halo becomes transparent to Mg II absorption. As f_M rises, more clouds are intercepted along lines-of-sight through the halo. As shown, different combinations of f_M and θ can result in a similar covering factor for strong Mg II absorption (see text).

properties of quasar haloes in terms of their expected ab-sorption signatures. In a recent work we have used pairs of quasars at different redshifts and investigated the presence of Mg II absorption around the foreground objects (Bowen et al. 2006). In 4/4 cases we have detected Mg II absorption with $W_0 > 0.5$Å in the spectrum of the background quasars with a redshift matching that of the foreground quasar. This suggests that strong Mg II absorbers are common in the transverse di-rection of quasars. We have extended our analysis to a larger sample of systems and our new results (Bowen et al. 2007) indicate that the presence of strong Mg II absorption around quasars with a covering factor close to unity within 100 kpc, with a rapid decline on larger scales. Such behavior is sim-ilar to that of Mg II gas which is detected around galaxies.

Interestingly, the high covering factor for Mg II gas in the transverse direction seem to be in contrast with smaller val-ues ($\sim 10\%$; Aldcroft et al. 1994) derived for Mg II absorp-tion along the line-of-sight to these objects (see Fig. 8). As we show below, this surprising finding is naturally explained by our model.

Quasar radiation is thought to be emitted into cones of opening angle θ (Antonucci 1993). As such, θ is a measure of the mass of cool gas within the halo which is exposed to the ionizing field and determines the mass of the remaining cool gas. The connection between θ and W_0 is therefore apparent within the framework of the model (see figure 8). Model pre-dictions for the absorption covering factor as a function of the

rest equivalent width, the impact parameter, and the mass of cool gas, f_M, are given in Fig. 9. These results are analogous to those of galaxies but for the additional dependence on θ. As shown, quasars that emit more isotropically have less cool gas at any impact parameter due to ionization effects. More massive envelopes of cool gas have a larger number of clouds and so result in broader Mg II troughs. Clearly, different combinations of f_M and θ can yield similar covering fractions. At present, neither the mass of cool gas in quasar halos nor the opening angle of quasar ionization cones are well determined with recent surveys indicating that of θ may depend on the quasar luminosity and is in the range $45° < \theta < 70°$ for bright quasars (Willott et al. 2000, Treister & Urry 2005). Fig. 9 shows that $f_M \simeq 5 - 10$ is required to explain the high occurrence of transverse strong Mg II absorption around quasars within 100 kpc in the Bowen et al. (2006, 2007) sample.

We can further compare the predictions of our model to observations by considering the fraction of quasars showing associated absorption, i.e. absorption arising along the quasar line-of-sight close to the quasar redshift (Fig. 8). As mentioned above, in such a case, low-ionization species are not expected to be abundant due to rapid ionizations by the quasar radiation field. However, the same clouds are expected to give rise to higher ionization absorption lines. In Fig. 10 we present predictions for the covering factor of H I, Mg II, C IV, and O VI lines as a function of halo mass and quasar quasar luminosity. The covering factor for all lines is seen to decrease exponentially with increasing W_0 due to Poisson statistics. As shown, the covering factor for absorption is more sensitive to the quasar luminosity than to the mass of cool gas in the halo. In particular, the halos of more luminous quasars are more ionized resulting in a lower covering factor for strong low ionization systems. As expected, more massive halos produce stronger absorption due to the larger number of clouds intercepted along the line-of-sight. Predictions appear to be in qualitative agreement with recent surveys indicating a covering factor of $\sim 30\%$ for strong C IV $\lambda\lambda 1548, 1550$ absorption (Vestergaard et al. 2003). Our model predicts little associated Mg II absorption due to halo gas. We note however, that our model does not include the, possibly important, contribution from absorption by gas in the immediate vicinity of the black hole (sometimes termed intrinsic absorption). That said, our model is consistent with the notion that most low ionization associated systems are intrinsic to the quasar. Additional data concerning the covering factor of various ionization stages as a function of quasar luminosity (and perhaps host mass) are required to test our model.

We note that a complementary configuration to the one used in the Bowen et al. (2006, 2007) survey is provided by radio galaxies. For these objects our line-of-sight passes outside the quasar radiation cone. Measurements of large-scale H I absorption by Van Ojik et al. (1997) have shown that typical column densities through the neutral part of the halo are of order $\lesssim 10^{19}$ cm^{-2}. Such values are in qualitative agreement with our model and with the Rao et al. (2006) dataset (see §2). A more detailed comparison is unwarranted at this stage.

3.3. *Quasar-halo emission properties*

As the gas is photo-excited by the radiation field of the quasar, clouds would not only absorb but also emit and scatter continuum and line photons. In this section we calculate the expected emission line flux from the halo.

Line emissivity depends on the ionization state of the gas as well as on the optical depth through which line photons need
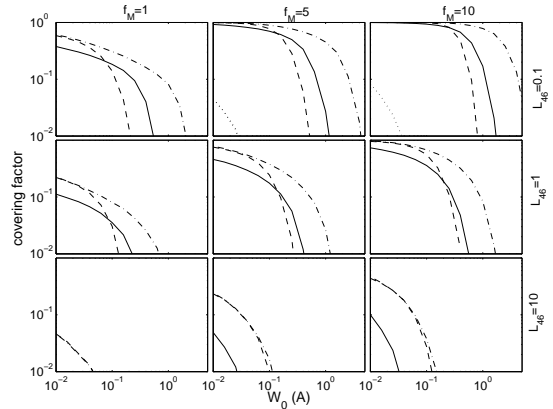

FIG. 10.— The predicted covering factor for associated absorption where lines-of-sight probe the ionized part of the halo. Covering factors for several high ionization lines are considered correspnding to: H I $\lambda 1216$ (dash-dotted line), Mg II $\lambda 2800$ (dotted line), C IV $\lambda 1548$ (solid line), and O VI $\lambda 1035$ (dashed line). The results are shown as a function of the quasar luminosity for $L_{46} = 0.1 - 10$ (columns) and mass in cold gas with $f_M = 1 - 10$. As shown, the covering factor is more sensitive to the luminosity rather than the mass in cold gas. The covering factor follows the exponential cutoff of the Poisson distribution for the respective lines. Low luminosity quasars have a higher covering factor for low ionization lines since the halo is less ionized. For bright objects the halo is more ionized and low ionization lines become weaker.

to propagate, escape, and reach the observer. In calculating the emissivity of lines we have assumed that once line photons escape individual clouds, they reach the observer; i.e., we assume no photon scattering or absorption among different clouds. This approximation is adequate if clouds along our line-of-sight have little overlap in velocity space, which is the case considered in this paper. The fraction of line photons escaping from a single cloud was calculated using CLOUDY using the escape probability method for a static cloud. The resulting emissivity per unit mass as a function of distance from the ionizing source is shown in Fig. 11 for Lyα emission line. As shown, averaged over volume, Lyα emissivity is relatively insensitive to the luminosity of the central object. This results from the gas temperature having only a weak dependence on luminosity for the relevant parameter range and from hydrogen being fully ionized. Emissivity is suppressed on small scales near very luminous sources due to suppression of the recombination rate at high ($\gg 10^5$ K) temperatures.

We have also studied the emissivity of other lines and, in particular, that of [O III] $\lambda 5007$ forbidden line (Fig. 11). The line emissivity in this case is very different from that of Lyα and other hydrogen-like lines since the recombination rate is much lower (O III and O IV abundances in the gas are negligible). Relatively neutral gas, which is required for efficient [O III] $\lambda 5007$ emission, becomes abundant only on large scales and even then only for relatively low luminosity quasars. As quasars get brighter the peak O III emissivity is shifted to larger scales where cooler gas is found. We emphasize that, unlike Lyα emission, [O III] $\lambda 5007$ emission is sensitive to gas composition and is roughly linear with it.

Our calculations allow us to predict how quasar halos would appear for different emission lines. We show an example for a Lyα image in Fig. 11 for the case of $\theta = 70°$, $f_M = 5$, $L_{46} = 1$ and assume that our line-of-sight is along the symmetry axis of the quasar. The image is symmetric with the surface brightness profile being roughly $\propto b^{-1}$ from the center (neglecting the effects of scattering; see below). We note that asymmetric images are obtained if the axis of symmetry is at an angle to

TABLE 2
EMISSION LINE PROPERTIES OF QUASAR NEBULAE

Line ID	L	Size	$\frac{L^{\text{scat,max}}}{L+L^{\text{scat,max}}}$
	[erg s^{-1}]	[kpc]	[ ]
H I Lyα	3×10^{43}	150	0.25
O VI $\lambda 1035$	4×10^{42}	80	0.25
N V $\lambda 1238$	2×10^{42}	150	0.25
C IV $\lambda 1548$	2×10^{42}	200	0.5
H I Hα	1×10^{42}	100	-
H I Hβ	8×10^{42}	150	-
C III $\lambda 977$	7×10^{41}	200	-
O VIII $\lambda 18.97$	4×10^{41}	20	?
[O III] $\lambda 5007$	2×10^{41}	200	-

Luminosities for doublets are the sum for individual transitions. Size is defined as the extent of the emitting nebula which contains 90% of the flux for a given transition. The last column is an order of magnitude estimate for the maximum luminosity in scattered light (see text). Transitions that do not scatter are marked with "-" while those for which the broad emission line flux is very uncertain are marked with "?" (see text). $L_{46} = 1$, $\theta = 70°$ and $f_M = 5$ are assumed.

our line-of-sight, as likely to be the case in general.

Different lines have different emissivity profiles and hence different luminosities and inferred nebular sizes. Table 2 lists a few of the more important lines which could, in principal, be observed in quasar haloes. Lyα, C IV $\lambda 1548$, and O VI $\lambda 1035$ are the strongest transitions with the latter two lines depending roughly linearly on the Metallicity. The typical nebular extent (from which most of the flux is emitted) of low ionization lines is > 100 kpc. This is in contrast to the apparent size of high ionization lines which come from compact, highly ionized regions of the halo (e.g., the nebular extent of O VIII X-ray lines is $\gtrsim 10$ kpc for $L_{46} = 1$).

3.3.1. Scattering

In addition to line emission there is scattering (i.e. absorption followed by emission) of the photons emitted by the quasar. Here broad emission line photons can be scattered off gas clouds in the halo provided the neutral hydrogen fraction is large enough. Owing to the low gas density, the population of excited levels is negligible and so only resonance lines are able to scatter efficiently. To correctly calculate the surface brightness profile due to photon scattering one requires detailed knowledge of the 3D distribution of clouds in real and velocity space. In addition, the fraction of photons reaching the halo depends on the amount of intrinsic absorption and the relative velocities of the emission line and halo gas. Detailed calculations should include the effect of multiple scatterings even in this relatively optically thin medium.

Despite the overall complexity of scattering problems, it is relatively straightforward to estimate the maximum scattered flux expected for different lines. This is simply the flux in the broad emission line with velocity dispersion, σ_l which is intercepted by halo clouds with velocity dispersion, σ_c given by roughly $\sigma_c/\sigma_l \simeq 10\%$ (here we used $\sigma_l \simeq 2000$; e.g., Vanden Berk et al. 2001). Given our quasar SED and taking the mean rest equivalent width for Lyα to be ~ 90Å (e.g., Zheng et al. 1997; Vanden Berk et al. 2001) we find that the the maximum scattered Lyα luminosity, $L_{\text{Ly}\alpha}^{\text{scat,max}} \sim 2 \times 10^{43} [1 - \sin(\theta)] L_{46}$ erg s^{-1}. Table 2 lists the results for other lines based on the same line-of-reasoning and shows that the contribution of scattered broad line region photons to the large scale nebular emission is probably less than 50% for all prominent lines (and for $L_{46} < 10^2$).

To better evaluate the flux due to broad emission line pho-

tons scattering off halo gas, we define an effective optical depth over the (dynamically broadened) absorption line profile of halo gas, $\tau_{\text{eff}}(r) = C(r)\tau(r)$ where $C(r)$ is the geometric covering factor of clouds at a given distance (i.e., the number of clouds intercepted at some distance interval) and $\tau(r)$ is the line optical depth of a single cloud at position r. In our model, $C(r)$ is large on small scales due to the clouds density peaking toward the center yet, $\tau(r)$, is low since the gas is more ionized. For Lyα, τ_{eff} is decreasing with decreasing r. On scales larger than ~ 30 kpc, clouds become opaque to Lyα and $\tau_{\text{eff}} \propto C \propto r^{-2}$. We have approximated the problem by running monte-carlo simulations (e.g., Zheng & Miralda-Escude 2002; Z. Zheng, private communication) of photons emitted by a point source and being scattered off halo gas with τ_{eff} being of order a few and having the radial dependence described above. We find that the surface brightness of the scattered photons is $\propto b^{-2.5}$ and therefore that most of the scattering occurs in the inner nebular regions (within ~ 30 kpc). The results are shown in the inset of Fig. 11 for the case of $L_{46} = 1$. We note, however, that these provide only order-of-magnitude estimates since the gas kinematics in the central regions of the halo is rather uncertain.

3.3.2. Detectability

It is interesting to examine the detectability of line emitting nebulae around quasars within the framework of our model. Here we focus on Lyα nebulosity and study its observed luminosity and size as a function of the limiting flux of the observation (see Fig. 12). As before, $f_M = 10$, $\theta = 70°$ and $L_{46} = 10$ are assumed. We also examine these quantities for several redshifts assuming the observed nebulae at those redshifts are similar so that the surface brightness is $\propto (1+z)^4$. Our calculations indicate that the limiting flux required to observe extended Lyα emission around $z = 1$ quasars is better than $\sim 10^{-16}$ erg s^{-1} cm^{-2} asec^{-2}. In particular, our model suggests that the observed nebular extent is sensitive to the limiting flux with a factor two increase in sensitivity allowing to detect emission from an order of magnitude larger volume. At low-z, a limiting flux of a few$\times 10^{-18}$ erg s^{-1} cm^{-2} asec^{-2} is required to probe the full extent of the nebulosity and correctly estimate its luminosity. Once the appropriate sensitivity is reached, our model suggests that large scale emission line nebulae in general, and Lyα nebulae in particular, should be a rather common phenomenon around quasars. More massive halos or quasars having a wider ionization cones are better emitters and their halos can be observed to higher-z. Our calculations suggest that Lyα scattering can have a substantial contribution to the observed luminosity (compare models B,C and D in figure 12). As expected, halos with lower mass of cool gas ($f_M = 1$) are poor emitters (compare models A and B in figure 12). Similar considerations also apply for metal lines whose detection can be used to put more stringent constraints on the ionization level of the emitting gas as well as estimate its mean metallicity. For example, the N V $\lambda 1238$ emission line could have a flux comparable to that of Lyα for $\gtrsim$solar metallicity gas (see table 2).

3.3.3. Comparison with observations

Extended narrow-line emission around quasars and radio galaxies has been observed for more than two decades and the accumulation of data has shown that giant Lyα nebulae
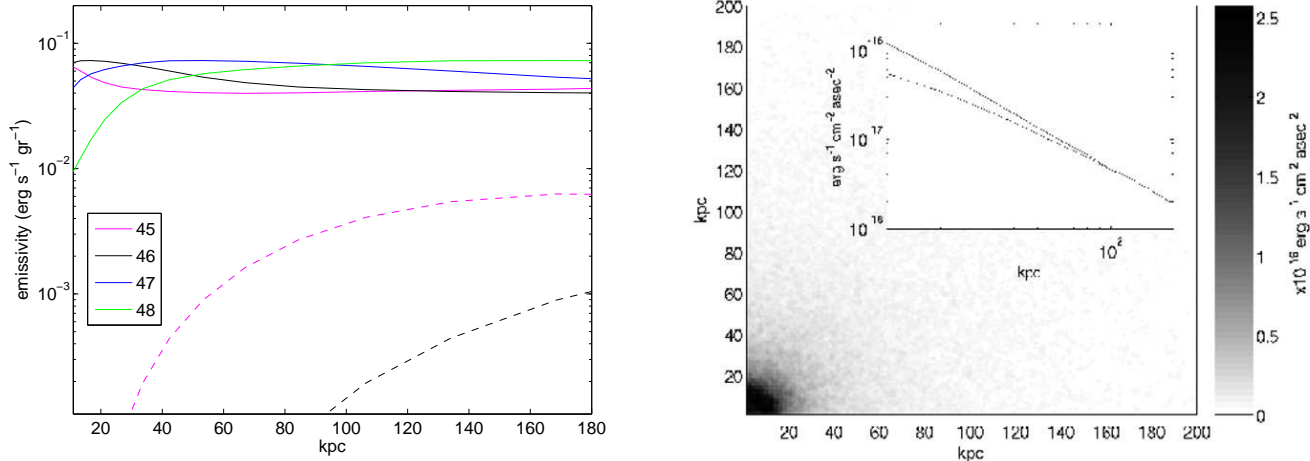
FIG. 11.— The Lyα (solid) and [O III] λ5007 (dashed) emissivities for various color coded luminosities. While the Lyα emissivities of the nebulae at large radii are similar, the emissivity decreases with increasing quasar luminosity on smaller, $\lesssim$ 30 kpc scales due to ionization effects. The [O III] λ5007 emissivities are lower than those of $L\alpha$ and have their maxima at larger radii where cool gas is more abundant. *Right:* The Lyα halo surrounding an $L_{46} = 1$ ($f_M = 5$, $\theta = 70°$) quasar at $z = 1$ with colors reflecting the flux level. Also shown in an inset is the surface brightness profile including (solid line) and excluding (dashed line) scattering of Lyα photons from the broad emission line region of the quasar (see text).

can be found around QSOs, up to scales of $\sim$ 100 kpc (e.g., Wampler et al. 1975, Stockton 1976, Bremer et al. 1992, Boroson, Oke, & Green 1982, Bergeron et al. 1983, Boroson, Persson, & Oke 1985, Stockton & MacKenty 1987, Reuland et al. 2003, Labiano et al. 2005). Early studies focused mostly on radio loud quasars but more recent ones showed that radio-quiet quasars also show extended Lyα emission on large scales. It is interesting to note that Hu et al. (1991) observed a sample of 7 radio-quiet quasars down to a limiting flux of 2×10^{-16}ergs^{-1}cm^{-2} and found no extended Lyα emission. However, subsequent and more sensitive observations showed that quasar nebulae are commonly observed around radio-quiet quasars (Weidinger et al. 2005, Bremer et al. 1992., Steidel et al. 1991, Hu et al. 1996, Petitjean et al. 1996). These authors report Lyα luminosities in the range $7 - 58 \times 10^{42}$ergs^{-1}, values which are largely consistent with our predictions as shown in Fig. 12. Christensen et al. (2006) report Lyα luminosities from $z \sim 3$ nebulae which are of order $\sim 10^{43}$ erg s^{-1} and extend up to a median value of 15 kpc (with some extending up to 60 kpc) for a flux limit of $\sim 10^{-17}$ erg cm^{-2} s^{-1} asec^{-2}. This is consistent with quasar halos having a considerable amount of gas in cool form (model A in figure 12 corresponding to $f_M = 1$ with no line scattering is excluded by the data; c.f. Binette et al. 2006). Christensen et al. place limits on C IV line emission down to fluxes ~ 10 times lower than Lyα. In our model this is roughly the predicted flux ratio of the lines for 0.1 solar metallicity. More detailed modeling is, however, beyond the scope of this paper.

The statistical properties of quasar halos and their underlying physics are poorly known and few models have been devised to account for them (e.g., Heckman et al. 1991). Common explanations for the existence of such line emission nebulae include gas accretion onto the central object (Haiman & Rees 2001) and matter ejection by the quasar and its host galaxy (e.g., Heckman et al. 1991). Moreover, the interpretation of the data is controversial: while several teams have reported high pressures of order $P \sim 10^{6-7}$cm^{-3} K for radio loud quasars (RLQ), a study by Fu & Stockton (2006) points to lower pressures, of order 10^4cm^{-3} K. These estimates

come from compact emission regions of [O II] and [O III] lines and from absorption by excited states (e.g., Hamann et al. 2001). In our model for the halo of an $L^\star$ galaxy the pressure is even lower, $P \sim$ a few$\times 10^2$ cm^{-3}. It is possible that RLQ are different from radio-quiet quasars (RQQ) given their overall higher Lyα luminosities (e.g., Christensen et al. 2006) and their apparently large X-ray and [OIII] emission on small scales (e.g., Crawford & Fabian 1989). Our model predicts relatively faint and diffuse [O III] emission from the halo which seems to be at odds with recent detections of [O II] and [O III] emitting filaments around RLQs. Deep optical observations of low-z RQQs may help to determine whether there is a relatively dense and filamentary structure in quasar halos in addition to the more diffuse component considered here.

4. DISCUSSION

4.1. *Galaxies*

Our model implies considerable mass in cool gas out to the virial radius of $L^\star$ galaxy halos at $z \sim 1$. As explained above, this assumes a unit covering factor for strong absorption within 50 kpc of the galaxy. The lower covering factors suggested by Bechtold & Ellingson (1992) and Tripp & Bowen (2005) would actually lead to an agreement between our model predictions and the results of Maller & Bullock (2004) who estimated the mass of cool gas in the Galaxy halo to be 2×10^{10} M$_\odot$ and argued for consistency with observations of high-velocity clouds. At present, radio surveys do not possess the required sensitivity to probe low column density, $\sim$ 100 kpc diffuse gas in 21 cm emission, as predicted by our model. We caution, however, that it is not clear whether our model predictions for $z \sim 1$ objects are directly applicable to present day galaxies. In particular, Nestor et al. (2005) find evidence for evolution of cool gas properties with cosmic time whereby the occurrence of strong systems appreciably declines from $z = 1$ to $z = 0.5$. Understanding the distribution of cool gas around present day galaxies will require extensive UV spectroscopic surveys.

The notion of massive galaxy halos has been promoted by Fukugita & Peebles (2006) to provide a solution to the missing baryon problem. In their model, the gas mass up to the
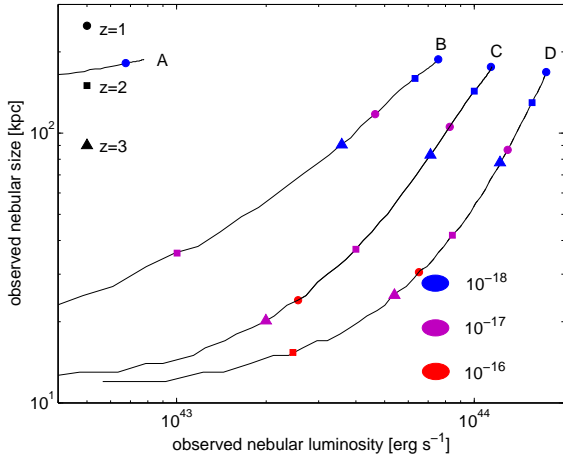
FIG. 12.— The observed Lyα nebula size (containing 90% of the total observed flux) vs. the observed luminosity for a halo illuminated by a $L_{46} = 10$ quasar with an opening angle $\theta = 70°$. The following models are considered: (A) $f_M = 1$ with no line scattering. (B) $f_M = 10$ with no line scattering. (C) $f_M = 10$ with scattered Lyα luminosity, $L_{Ly\alpha}^{scat} = 0.5 L_{Ly\alpha}^{scat,max}$. (D) $f_M = 10$ and $L_{Ly\alpha}^{scat} = L_{Ly\alpha}^{scat,max}$. We assume no evolution in the nebular properties with redshift. Placing the same nebula at different redshifts (denoted by different symbols; see legend) decreases its observed luminosity and size for a survey with a given limiting flux (denoted by colors in units of erg s^{-1}cm^{-2}asec^{-2}). Clearly, unless the nebula is close and/or the sensitivity is high, only the brighter inner part of the nebula is observed which results in an under-estimation of its luminosity and size (see text). In particular, sensitivities of order 10^{-18} erg s^{-1}cm^{-2}asec^{-2} are required to probe the full extent of quasar nebulae at $z \lesssim 2$ (blue square and circle).

virial radius is a few$\times 10^{11}$ M$_\odot$. Their total gas mass estimates provide a natural explanation to the missing baryon problem and are consistent with a large range of observational constraints which are independent of those considered here. Their model did not consider the possible existence of cool gas beyond the extent of the disk. Here we have shown that converting a fraction of the hot plasma into cool clumps allows us to reproduce a number of observational constraints from absorption line studies, while not significantly changing the total amount of gas within the virial radius (see Fig. 5).

More work is needed to establish how much mass there is in the halos of present day galaxies. On the observational side, better estimates of the covering fraction of cool gas around galaxies are required, possibly as a function of galaxy type. On the theoretical side, numerical simulations of galaxy formation need to include realistic cooling rates and reach high resolutions to reliably trace cool and condensed forms of gas. Understanding the properties of the dilute and ellusive, yet likely very massive, cool gas component in galaxy halos is essential for understanding galaxy formation and evolution from the early Universe, to present times and beyond.

4.2. *Quasars*

Quasars are known to reside in galaxies yet their large scale environments are poorly understood. The recent discovery of Mg II absorbing gas around those objects (Bowen et al. 2006, 2007) suggests an interesting link between galaxy and quasar environments. This implies that the presence of a quasar can be used to shed light on the distribution of matter in the halos of galaxies.

We have shown that it is possible to construct a model which unifies several distinct astrophysical phenomena pertaining to intervening absorption, associated absorption, and

quasar emission nebulae. In our model, these phenomena are different manifestations of the same physical entity, that being of cool gas condensations distributed within the halo of galaxies. If our model is correct then the properties of cool gas in the vicinity of galaxies may be revealed by studying the influence of an active nucleus on its thermal and ionization structure. In particular, the study of associated absorption may help to constrain the density and distance of halo gas from the quasar. Cool gas around galaxies is notoriously difficult to detect in emission. Nevertheless, the presence of an ionizing source enhances emission and renders the detection of circum-galactic material more accessible. Furthermore, by studying the nebulosities around quasars, one can obtain a 2D-spatial×1D-velocity picture of the gas. Mean quantities pertaining to the mass of the gas and its metallicity can be more easily deduced for individual objects.

In addition to shedding light on gas distribution in the halos of galaxies, it is possible to deduce important conclusions about quasar physics: the recent results by Bowen et al. (2006, 2007) indicate a covering factor of order unity for cool gas in the transverse direction around quasars in contrast to the much lower covering factor for associated Mg II absorption. Our model implies that this is merely a consequence of the quasar unification scheme: gas in the radial direction to the quasar is heated to high temperatures while that which is at right angles to the quasar ionization cone remains unaffected. This is not a trivial result since, although the unification scheme is well established for active galactic nuclei, it is less secure for bright quasars at high-z. Further tests of this conjecture may be carried out by comparing model predictions to the occurrence of associated absorbers for a wide range of ionization levels as well as by studying emission line nebulae in detail.

Our model can reproduce the emission and absorption properties of quasars by requiring quasar halos to be more extended and therefore more massive than those of $L^\star$ galaxies (c.f. Serber et al. 2006). Such a scaling combined with the radiation properties of quasars can simultaneously explain the anisotropic absorption properties and the Lyα nebulae observed on scales reaching ~ 100 kpc. Finally, if the correlation found between the size of cool gaseous halos and galaxy luminosity (Steidel et al. 1997, Guillemin & Bergeron 1997) can be extended to quasars then this implies that quasar hosts are a few$\times L^\star$, which is in agreement with results from Jahnke et al. (2004).

Better understanding of quasar emission line nebulae may allow us to deduce the long-term light-curve behavior of quasars. This will require better understanding of the matter distribution in quasar halos which can be achieved by deep imaging and spatially resolved spectroscopy of quasar environments. The detection of orphan nebulae (where the active nucleus is obscure) may provide a new means for identifying type-II quasars. Combining large samples of emitting and absorbing gaseous nebulae may allow us to statistically constrain the mass of cool gas in quasar halos as well as the opening angle of quasars. This has implications for re-ionization and background radiation determination. A survey of emission line nebulae around a large number of quasars may also reveal environmental differences among quasar types (e.g., the RQQ-RLQ dichotomy).

The detection of metal emission lines, whose presence (depending on the gas composition) is predicted by our model, may allow to estimate the metallicity of gas in the halo and test models for metal enrichment of galaxies and the inter-

galactic/intra-cluster medium.

5. SUMMARY

We have presented a phenomenological model for the distribution of cool gas around $L^\star$ galaxies, calibrated with a wide range of observational constraints from absorption line studies (rest equivalent width distribution of Mg II absorbers, HI column density, etc.). We argue that the halos of $L^\star$ galaxies are filled with gaseous clouds with sizes of order 1 kpc, masses of $\sim 10^6 M_\odot$ and particle densities $\sim 10^{-2} \mathrm{cm}^{-3}$. The total amount of cool gas within the virial radius of $L^\star$ galaxies depends on the covering factor for strong Mg II absorption (which is a matter of debate) and is likely to be in the range $10^{10} < M_{\mathrm{cool}} < 10^{11} M_\odot$, within the virial radius.

By assuming self-similarity, we show that the obtained solution for the distribution of cool gas around galaxies, if appropriately scaled, can reproduce the properties of cool gas

seen quasars. Our model simultaneously provides an explanation for the Lα nebulosities observed observed on ~ 100 kpc scales around quasars as well as the main properties of the cool gas seen in absorption around quasars.

Comparison of model predictions with future surveys will shed light on the missing baryon problem and will deepen our understanding with respect to galaxy formation and quasar activation.

APPENDIX

Here we describe the time-dependent ionization and thermal structure of an initially cool cloud which is exposed to a quasar's ionizing radiation. As the quasar phenomenon is short lived compared to the Hubble time (the quasar lifetime, $\tau_q \sim 10^7$ years; e.g., Worseck & Wisotzki 2006), it is instructive to first consider a few relevant timescales of the problem:

- The dynamical timescale of a halo of size R_{halo} at a virial temperature, T_v (corresponding to some sound speed, v_s) is

$$\tau_{\mathrm{dyn}} \sim \frac{R_{\mathrm{halo}}}{v_s} \simeq 10^9 \frac{r}{100\,\mathrm{kpc}} \left(\frac{T_v}{10^7 \mathrm{K}}\right)^{-1/2} \mathrm{yr} \tag{1}$$

- The sound crossing timescale for a cloud of size $2R_{\mathrm{cloud}}$ at temperature T is

$$\tau_{\mathrm{cross}} \sim \frac{2R_{\mathrm{cloud}}}{v_s} \simeq 10^8 \frac{R_{\mathrm{cloud}}}{1\,\mathrm{kpc}} \left(\frac{T}{10^4 \mathrm{K}}\right)^{-1/2} \mathrm{yr} \tag{2}$$

- The photoionization timescale for ion X is

$$\tau_{\mathrm{ion}}^X = \left(\int \frac{\sigma_X(E) L_E}{4\pi r^2 E} dE\right)^{-1} \sim 10^3 L_{46}^{-1} \left(\frac{r}{10^2 \mathrm{kpc}}\right)^2 \mathrm{yr} \tag{3}$$

where σ_X is the cross-section, E the energy, L_E the flux per unit energy, r the distance from the quasar. We assumed a mean ionizing photon energy of $E = 10\,\mathrm{eV}$ and an ionization cross-section of 10^{-19} cm^2 (roughly that of Mg II).

- The recombination timescale for ion X is

$$\tau_{\mathrm{rec}}^X = \frac{1}{n\alpha_X(T)} \sim 5 \times 10^4 \left(\frac{n}{0.02\mathrm{cm}^{-3}}\right)^{-1} \mathrm{yr} \tag{4}$$

where n is the number density of atoms and α_X the recombination coefficient (taking only the radiative term for Mg II).

The photoionization and recombination timescales are the shortest in the problem. The cloud and halo dynamical timescales (approximated by the sound-crossing time) are probably longer than the quasar lifetime, τ_q; hence, while the ionization structure of the clouds can vary rapidly (see below), the structure of the halo and embedded clouds remains approximately constant during the quasar lifetime. We note, however, that the sound-crossing timescale for the smallest clouds in our model could be as short as $\sim 10^7$ years if their temperature rises to high values once the quasar activates. We choose to ignore this complication here since (a) the quasar lifetime is poorly known and (b) the evaporation timescale is a few times the sound-crossing timescale (e.g., Bertoldi 1989). Also, due to the spectrum of the cloud's size-distribution, the evaporation of the smallest clouds will make little difference to our final conclusions.

In addition to the above analytic approximations, we have numerically computed several time-dependent photoionization and thermal models. This is necessary to quantify just how important the effects of the varying quasar flux are compared to time independent calculations and to see which ions are affected most. The algorithm used for these calculations is fully described in Gnat & Sternberg (2006).

At the beginning of the calculation we assume that the cloud is exposed to the meta-galactic field and is in ionization and thermal equilibrium. We then turn on a quasar and assume a step function description for its light curve, i.e., the quasar if off for $t < 0$ and on at $t \geq 0$. The quasar is assumed to maintain a constant flux level to $t \to \infty$. The calculations are carried out under isochoric conditions, as appropriate given the above considerations.
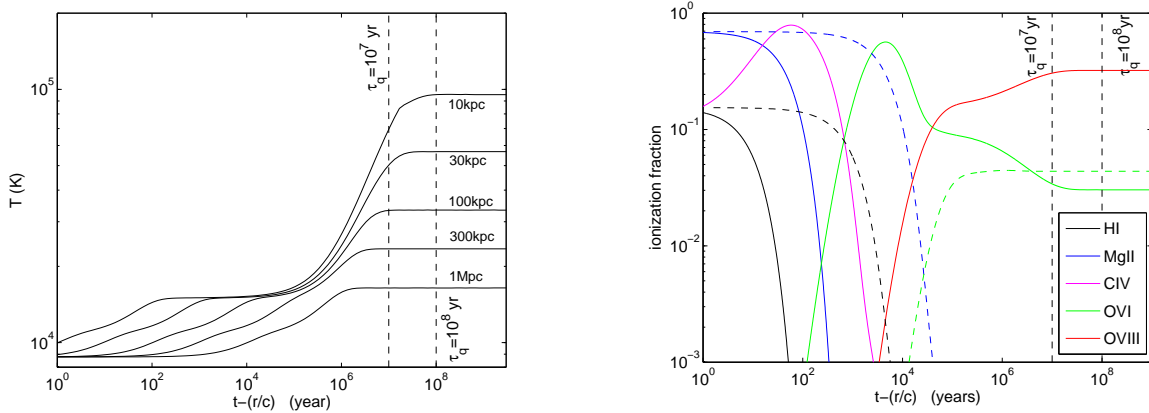
FIG. 13.— Time dependent thermal structure of the halo after a quasar ignites at $t = 0$ (and a cloud at a distance r from it is then exposed at time $t + r/c$) assuming $L_{46}(t) = \Theta(t)$ where $\Theta(t)$ is a step function. Also plotted are estimates for typical quasar lifetimes. Time dependent photoionization effects are important and prevent the gas from reaching very high temperatures (close to the Compton temperature) over the quasar lifetime. *Right:* Ionization fractions for several abundant elements as a function of time. Colors denote different ions (see legend) while different lines denote gas at different distances from the quasars: 30 kpc (solid), and 300 kpc (dashed) lines. The rapid ionization of all low level ions is clearly seen and takes place over $\lesssim 10^4$ years. Such gas will therefore disappear from the line-of-sight and would become transparent. We note the general agreement between the ionization timescales obtained and the analytic approximation (equation A3).

The thermal calculations are shown in Fig. 13 for the case of $L_{46} = 1$, and demonstrate the limitations of the assumption of photoionization and thermal equilibrium. The gas heats up very quickly near the quasar where the ionizing flux is high and less so on larger scales. Typically, the gas within the inner 50 kpc heats up to $\sim 2 \times 10^4$ K over a period of $\sim 10^4$ years (cf. equations A3,A4). Further heating occurs on somewhat longer timescales which can be comparable to the quasar lifetime. Unless one happens to intercept young quasars then the inner 50 kpc region of the halo would be heated to $\lesssim 10^5$ K over the quasar lifetime. We conclude that, for moderate luminosity quasars, the gas in the central regions of the haloes can be efficiently heated to $\lesssim 10^5$ K. Nevertheless, further heating is delayed and may take longer than the quasar duty-cycle or other relevant dynamical timescales of the problem. Assuming τ_q is similar for all quasars then higher temperatures can be reached in the inner regions of the haloes of bright quasars since the ionization timescale is shorter and the flux higher.

We have also calculated the time-dependent ionization structure of the halo and trace several of the ionization levels in Fig. 13. As shown, all the low ionization stages usually probed by absorption line studies quickly attain negligible abundances and are not likely to be observed unless the quasar brightened over short timescales. For example, Mg II and H I would be immediately ionized and the gas is quickly heated. Time-dependent ionization deviations from a steady-state solution can be important but mainly for the high ionization levels whose absorption lines would appear in the X-ray region of the quasar spectrum.

The above analysis suggests that it may be possible to treat the halos of quasars as having the same structure as galaxy halos since little structural changes are likely to occur over the quasar lifetime by radiation effects alone. We note that this is may not be the case if quasar activity is a recurring phenomenon or if they have additional means of affecting their environment (e.g., via jets, winds, etc.). To conclude, for the purpose of this work, steady-state photoionization calculations can be adequately used to describe the ionization and thermal state of the halo gas at all times.

REFERENCES

Antonucci, R. 1993, ARA&A, 31, 473
Badnell, N. R. 2006, A&A, 447, 389
Bahcall, J. N., & Spitzer, L. J. 1969, ApJ, 156, L63
Bechtold, J., & Ellingson, E. 1992, ApJ, 396, 20
Bergeron, J., Dennefeld, M., Boksenberg, A., & Tarenghi, M. 1983, MNRAS, 202, 125
Bergeron, J. 1986, A&A, 155, L8
Bergeron, J., & Stasinska, G. 1986, A&A, 169, 1
Bergeron, J., Kunth, D., & D'Odorico, S. 1987, A&A, 180, 1
Bergeron, J., & Durret, F. 1987, A&A, 184, 93
Bergeron, J., & Boisse, P. 1991, A&A, 243, 344
Bergeron, J., & Herbert-Fort, S. 2005, IAU Colloq. 199: Probing Galaxies through Quasar Absorption Lines, 265
Bertoldi, F. 1989, ApJ, 346, 735
Binette, L., Wilman, R. J., Villar-Martín, M., Fosbury, R. A. E., Jarvis, M. J., Röttgering, H. J. A. 2006, A&A, 459, 31
Bland-Hawthorn, J., & Maloney, P. R. 2001, ApJ, 550, L231
Boroson, T. A., Oke, J. B., & Green, R. F. 1982, ApJ, 263, 32
Boroson, T. A., Persson, S. E., & Oke, J. B. 1985, ApJ, 293, 120
Bowen, D. V., Blades, J. C., & Pettini, M. 1995, ApJ, 448, 634
Bowen, D. V., et al. 2006, ApJ, 645, L105
Bowen, D. V., et al. 2007, ApJ, submitted
Bremer, M. N., Fabian, A. C., Sargent, W. L. W., Steidel, C. C., Boksenberg, A., & Johnstone, R. M. 1992, MNRAS, 258, 23P
Bruzual A., G., & Charlot, S. 1993, ApJ, 405, 538
Chabrier, G. 2003, PASP, 115, 763

Charlton, J. C., Mellon, R. R., Rigby, J. R., & Churchill, C. W. 2000, ApJ, 545, 635
Cristiani, S. 1987, A&A, 175, L1
Christensen, L., Jahnke, K., Wisotzki, L., & Sánchez, S. F. 2006, A&A, 459, 717
Churchill, C. W., Mellon, R. R., Charlton, J. C., Jannuzi, B. T., Kirhakos, S., Steidel, C. C., & Schneider, D. P. 2000, ApJS, 130, 91
Churchill, C. W., & Vogt, S. S. 2001, AJ, 122, 679
Churchill, C. W., Vogt, S. S., & Charlton, J. C. 2003, AJ, 125, 98
Churchill, C. W., Kacprzak, G. G., & Steidel, C. C. 2005, IAU Colloq. 199: Probing Galaxies through Quasar Absorption Lines, 24
Crawford, C. S., & Fabian, A. C. 1989, MNRAS, 239, 219
Crenshaw, D. M., Kraemer, S. B., & George, I. M. 2003, ARA&A, 41, 117
Danforth, C. W., & Shull, J. M. 2005, ApJ, 624, 555
Ding, J., Charlton, J. C., Churchill, C. W., & Palma, C. 2003, ApJ, 590, 746
Ellison, S. L., Ibata, R., Pettini, M., Lewis, G. F., Aracil, B., Petitjean, P., & Srianand, R. 2004, A&A, 414, 79
Ferland, G. J., Korista, K. T., Verner, D. A., Ferguson, J. W., Kingdon, J. B., & Verner, E. M. 1998, PASP, 110, 761
Fu, H., & Stockton, A. 2006, ApJ, 650, 80
Fukugita, M., & Peebles, P. J. E. 2006, ApJ, 639, 590
Gehrels, N. 1986, ApJ, 303, 336
Gnat, O., & Sternberg, A. 2004, ApJ, 608, 229
Gnat, O., & Sternberg, A. 2006, ApJ, accepted
Guillemin, P., & Bergeron, J. 1997, A&A, 328, 499
Haardt, F., & Madau, P. 1996, ApJ, 461, 20

Haiman, Z., & Rees, M. J. 2001, ApJ, 556, 87
Hamann, F. W., Barlow, T. A., Chaffee, F. C., Foltz, C. B., & Weymann, R. J. 2001, ApJ, 550, 142
Heckman, T. M., Miley, G. K., Lehnert, M. D., & van Breugel, W. 1991, ApJ, 370, 78
Heckman, T. M., Lehnert, M. D., Miley, G. K., & van Breugel, W. 1991, ApJ, 381, 373
Heckman, T. M., Sembach, K. R., Meurer, G. R., Leitherer, C., Calzetti, D., & Martin, C. L. 2001, ApJ, 558, 56
Hu, E. M., Songaila, A., Cowie, L. L., & Stockton, A. 1991, ApJ, 368, 28
Hu, E. M., McMahon, R. G., & Egami, E. 1996, ApJ, 459, L53
Jahnke, K., & Wisotzki, L. 2003, MNRAS, 346, 304
Jahnke, K., Kuhlbrodt, B., & Wisotzki, L. 2004, MNRAS, 352, 399
Kacprzak, G. G., Churchill, C. W., Steidel, C. C., Murphy, M. T., & Evans, J. L. 2007, ApJ, 662, 909
Krolik, J. H., & Kriss, G. A. 2001, ApJ, 561, 684
Labiano, A., et al. 2005, A&A, 436, 493
Lanzetta, K. M., & Bowen, D. 1990, ApJ, 357, 321
Lanzetta, K. M., Bowen, D. V., Tytler, D., & Webb, J. K. 1995, ApJ, 442, 538
Maller, A. H., & Bullock, J. S. 2004, MNRAS, 355, 694
Martin, C. L. 2006, ApJ, 647, 222
McKee, C. F., & Begelman, M. C. 1990, ApJ, 358, 392
Ménard et al. 2007, ApJ, submitted (astro-ph/0706.0898)
Mo, H. J., & Miralda-Escude, J. 1996, ApJ, 469, 589
Nestor, D. B., Turnshek, D. A., & Rao, S. M. 2005, ApJ, 628, 637
Norman, C., et al. 2004, ApJ, 607, 721
Oppenheimer, B. D., & Davé, R. 2006, MNRAS, 373, 1265
Petitjean, P., & Bergeron, J. 1994, A&A, 283, 759
Petitjean, P., Pécontal, E., Valls-Gabaud, D., & Chariot, S. 1996, Nature, 380, 411
Prochaska, J. X., & Wolfe, A. M. 1997, ApJ, 487, 73
Prochaska, J. X., & Wolfe, A. M. 1998, ApJ, 507, 113
Prochter, G. E., Prochaska, J. X., & Burles, S. M. 2006, ApJ, 639, 766
Ptak, A., Zakamska, N. L., Strauss, M. A., Krolik, J. H., Heckman, T. M., Schneider, D. P., & Brinkmann, J. 2006, ApJ, 637, 147
Ranalli, P., Comastri, A., & Setti, G. 2003, A&A, 399, 39
Rao, S. M., Turnshek, D. A., & Nestor, D. B. 2006, ApJ, 636, 610
Rauch, M., Sargent, W. L. W., Barlow, T. A., & Simcoe, R. A. 2002, ApJ, 576, 45
Reuland, M., et al. 2003, ApJ, 592, 755

Sazonov, S. Y., Ostriker, J. P., & Sunyaev, R. A. 2004, MNRAS, 347, 144
Serber, W., Bahcall, N., Ménard, B., & Richards, G. 2006, ApJ, 643, 68
Steidel, C. C., & Sargent, W. L. W. 1992, ApJS, 80, 1
Steidel, C. C. 1993, ASSL Vol. 188: The Environment and Evolution of Galaxies, 263
Steidel, C. C., Dickinson, M., & Persson, S. E. 1994, ApJ, 437, L75
Steidel, C. C., Dickinson, M., Meyer, D. M., Adelberger, K. L., & Sembach, K. R. 1997, ApJ, 480, 568
Steidel, C. C., Kollmeier, J. A., Shapley, A. E., Churchill, C. W., Dickinson, M., & Pettini, M. 2002, ApJ, 570, 526
Sternberg, A., McKee, C. F., & Wolfire, M. G. 2002, ApJS, 143, 419
Stockton, A. 1976, ApJ, 205, L113
Stockton, A., & MacKenty, J. W. 1987, ApJ, 316, 584
Stockton, A., MacKenty, J. W., Hu, E. M., & Kim, T.-S. 2002, ApJ, 572, 735
Treister, E., & Urry, C. M. 2005, ApJ, 630, 115
Turnshek, D. A., Rao, S. M., Nestor, D. B., Belfort-Mihalyi, M., & Quider, A. M. 2005, IAU Colloq. 199: Probing Galaxies through Quasar Absorption Lines, 104 (astro-ph/0506701)
van Ojik, R., Roettgering, H. J. A., Miley, G. K., & Hunstead, R. W. 1997, A&A, 317, 358
Vanden Berk, D. E., et al. 2001, AJ, 122, 549
Vestergaard, M. 2003, ApJ, 599, 116
Wampler, E. J., Burbidge, E. M., Baldwin, J. A., & Robinson, L. B. 1975, ApJ, 198, L49
Weidinger, M., Møller, P., Fynbo, J. P. U., & Thomsen, B. 2005, A&A, 436, 825
Willott, C. J., Rawlings, S., Blundell, K. M., & Lacy, M. 2000, MNRAS, 316, 449
Worseck, G., & Wisotzki, L. 2006, A&A, 450, 495
York, D. G., Dopita, M., Green, R., & Bechtold, J. 1986, ApJ, 311, 610
York, D. G., et al. 2006, MNRAS, 367, 945
Zheng, W., Kriss, G. A., Telfer, R. C., Grimes, J. P., & Davidsen, A. F. 1997, ApJ, 475, 469
Zheng, Z., & Miralda-Escudé, J. 2002, ApJ, 578, 33
Zibetti, S., Ménard, B., Nestor, D., & Turnshek, D. 2005, ApJ, 631, L105
Zibetti, S., Ménard, B., Nestor, D., & Turnshek, D. 2006, ApJ, in press
Zwaan, M. A., van der Hulst, J. M., Briggs, F. H., Verheijen, M. A. W., & Ryan-Weber, E. V. 2005, MNRAS, 364, 1467